Control of micro-CHP and thermal energy storage for minimising electrical grid utilisation

John Allison[1]*, Gavin Bruce Murphy[1] and John Mark Counsell[2]
[1]*Mechanical & Aerospace Engineering, University of Strathclyde, Glasgow, UK;*
[2]*Electrical Engineering & Electronics, University of Liverpool, Liverpool, UK*

Abstract

The efficient use of combined heat and power (CHP) systems in buildings presents a control challenge due to their simultaneous production of thermal and electrical energy. The use of thermal energy storage coupled with a CHP engine provides an interesting solution to the problem—the electrical demands of the building can be matched by the CHP engine, while the resulting thermal energy can be regulated by the thermal energy store. Based on the thermal energy demands of the building the thermal store can provide extra thermal energy or absorb surplus thermal energy production. This paper presents a multi-input multi-output inverse-dynamics-based control strategy that will minimise the electrical grid utilisation of a building, while simultaneously maintaining a defined operative temperature. Electrical demands from lighting and appliances within the building are considered. In order to assess the performance of the control strategy, a European Standard validated simplified dynamic building physics model is presented that provides verified heating demands. Internal heat gains from solar radiation and internal loads are included within the model. Results indicate the control strategy is effective in minimising the electrical grid use and maximising the utilisation of the available energy when compared with conventional heating systems.

Keywords: control systems; energy storage; combined heat and power; energy conservation.

*Corresponding author:
j.allison@strath.ac.uk

Received 10 July 2013; revised 6 June 2014; accepted 25 June 2014

1 INTRODUCTION

The built environment has an extensive contribution to the global production of carbon emissions and energy use. It has been stated that the built environment accounts for as much as 50% of the energy requirement of the UK [1]. The commercial sector similarly accounts for 40% of resource consumption in the European Union [2]. The World Business Council for Sustainable Development's 4 year, $15 million Energy Efficiency in Buildings research project [3] has concluded that buildings account for 40% of global energy consumption. As such commercial buildings are a key target for carbon reduction measures. One method of reducing commercial buildings' energy consumption is to make them more autonomous—creating more of their own energy, disposing of their own waste, collecting their own water; ultimately being as sustainable as possible (i.e. self-sustaining). In the drive to reduce energy used by commercial buildings and to move towards more sustainable and less grid-dependant offices, the method of meeting electrical and thermal demand is of the utmost importance.

Combined heat and power (CHP) systems offer an alternative to more traditional heating systems, with the main difference being that they produce both thermal and electrical energy. CHP systems are highly efficient due to the utilisation of the heat produced during operation. Thermal energy storage coupled with CHP will become especially important as demand for hot water will dominate in buildings which have low heat loss and meet advanced building standards such as Passivhaus [4, 5]. Previous work highlights the reduction of emissions which can be achieved with CHP systems installed in various commercial buildings [6]. Thermal energy storage offers greater flexibility for a building with a CHP system as the thermal store provides extra thermal capacity which can help to regulate demand from the primary source. A method to help size a thermal store for a building with a CHP system is introduced here that confirms the importance of correctly sizing a thermal energy store. A CHP

International Journal of Low-Carbon Technologies 2016, 11, 109–118

doi:10.1093/ijlct/ctu023 Advance Access Publication 21 August 2014

system with thermal energy storage requires implementation of a robust controller design strategy to optimise operation and minimise energy use.

Office buildings are also ideal for utilising photovoltaic (PV) systems since they generate carbon-free electricity during the main periods of electrical demand. However, matching the dynamic availability of PV systems with the power generation from an electrically-led CHP engine can be difficult.

Therefore, a multi-input multi-output (MIMO) control strategy is presented which is designed to minimise the electrical grid utilisation of a building, while simultaneously maintaining a defined operative temperature. This is achieved through control of the CHP engine and thermal energy store while dynamically compensating for availability of PV, and changes in climate. A full control strategy is also given for the case where electrical energy storage is available, but is not considered in the analysis given.

Controllability of buildings and their heating systems are key for both energy reduction and occupant comfort [7]. To develop and present the MIMO control strategy, a simplified dynamic building model has been developed. The model and its validation process are presented. The building model is underpinned by a holistic approach to the mathematical modelling of the dynamics of a building and its systems. This model is used to analyse the controllability of a building using a nonlinear inverse dynamics-based controller design methodology used in the aerospace and robotics industry.

2 METHODOLOGY

The methodology comprises two main sections: the presentation of an EN 15265 validated dynamic building model and the subsequent implementation of an idealised control strategy for a micro-CHP plant and thermal energy store within the model.

The model has been validated with the European Standard for the energy performance of buildings [8]. This standard can be used to ensure that the calculation of energy needs for space heating and cooling of a zone in a building, computed by a model, are accurate. This is important as accurate energy data should be used for analysing the controller performance. This is essential for this controller design as the sizing of the CHP plant and thermal energy store is critical, and should also be in line with possible real world installations for the building zone considered.

The models of the thermal energy store and CHP plant are idealised, nonlinear, energy-based models that are used as a proof-of-concept and are considered sufficient for system performance analysis. The controller design employed is an inverse dynamics-based MIMO controller.

2.1 Building model

The building model presented is an extension of a previously published [9] building physics model that has been calibrated with empirical data for residential dwellings. This iteration of the model comprised five ordinary differential equations (ODEs) that represents the convective and radiative heat transfer between the five temperature nodes and the outside environment. The zone is considered a closed space delimited by enclosure elements. The five nodes were chosen to represent the air within the zone and each of the enclosure elements:

- Air temperature, T_a
- Internal wall temperature, T_{iw}
- Roof/ceiling temperature, T_r
- Floor temperature, T_f
- Structural wall temperature, T_s.

Numerous heat transfer mechanisms between the nodes are accounted for in the model. Heat is transferred to and from the components by radiation interchange with other components and by convective heat transfer between the air and the components.

Heat transfer occurs through the building envelope: via the glazing, roof and structure using thermal transmittance values; via natural infiltration through gaps and cracks and via ventilation using external air.

The solar radiation incident on the external envelope that is transferred into the zone is accounted for using the solar energy transmittance of each element. A fraction of this solar radiation is immediately delivered to the internal air, while the rest is absorbed by the internal surface of each component. The extra heat flow due to the thermal radiation to the sky from each external component is included in the solar heat gain calculation.

The convective and radiative heat transfer from the internal loads (lighting, people and IT equipment) is also accounted for. The convective portion affects the air temperature immediately, while the radiative portion is distributed between the walls and floor.

Finally, the heat transfer for the heating or cooling load required (positive for heating and negative for cooling) is supplied to, or extracted from, the internal air node.

The mechanisms of heat transfer between the nodes can be represented in a generalised thermal resistance–capacitance network for the single zone building model. The convective and radiative heat transfer networks are given in Figure 1. It should be noted that the thermal capacities of each node along with the distribution of the solar and internal load heat flows have been excluded from these figures for clarity.

There are a number of basic assumptions used for this dynamic calculation method that are in line with those accepted by the European Standard. These include but are not limited to the following: (a) the air temperature is uniform throughout the room; (b) the thermophysical properties of all materials are constant and isotropic; (c) the heat conduction through the components is one dimensional; (d) the distribution of the solar radiation on the component surfaces is fixed and (e) the radiative heat flow is uniform over the surface of the components. These assumptions allow the model to be simplified but still retain enough complexity to ensure accurate energy requirement calculation.

By following the thermal network in Figure 1 it is possible to construct the five ODEs that the model comprises. These are

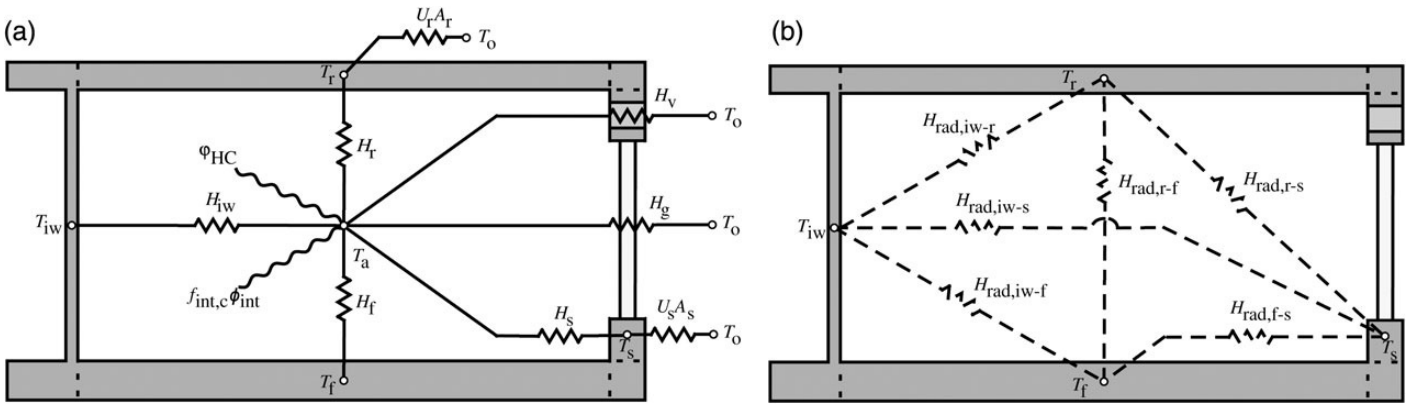

Figure 1. *Heat transfer resistance network: (**a**) convective and (**b**) radiative.*

given as Equations (A1)–(A5) in Appendix A.1. In order to solve this set of ODEs, they are implemented within the MATLAB® environment in a state-space form. The equations are then numerically integrated to calculate the required heating or cooling load at each time step of the simulation.

2.2 Model validation

Validation of the model with the European Standard requires the comparison of yearly calculated results for both heating and cooling loads with given reference values over eight test cases. There are an additional four test cases that are not mandatory, these are provided as informative tests in order to check the basic operation of a calculation method.

The zone modelled is a small office located in Trappes, France for which the climatic data (external air temperature and solar radiation) are provided. Figure 2 shows the wire-frame drawing of the office zone modelled, with major dimensions indicated. Additionally, the thermophysical properties such as layer thickness (d, in m) design thermal conductivity (λ, in W/(m K)), density (ρ, in kg/m^3) ρ, specific heat capacity (c_p, in J/(kg K)), of each layer of the opaque building components (external wall, internal walls, roof/ceiling and floor) are also provided for each of the test cases. There is ventilation (1 air change per hour) by external air between 08:00 and 18:00 during weekdays. The internal gains are set at 20 W/m^2 and are defined as 100% convective to the internal air of the zone. The heating and cooling is intermittent and are only in effect from 08:00 to 18:00 during weekdays. The set point for heating is 20°C and cooling is 26°C, using air temperature as the controlled variable.

For each of the test cases, a major element of the building model is changed in order to assess the model's performance. These involve changing the inertia of the building, removing the internal gains, altering the solar protection and adding an external roof. Full details of each test case can be found in the Standard.

Although much of the required input data are given in the Standard, there are several parameters that have to be calculated based on the thermophysical properties of the building

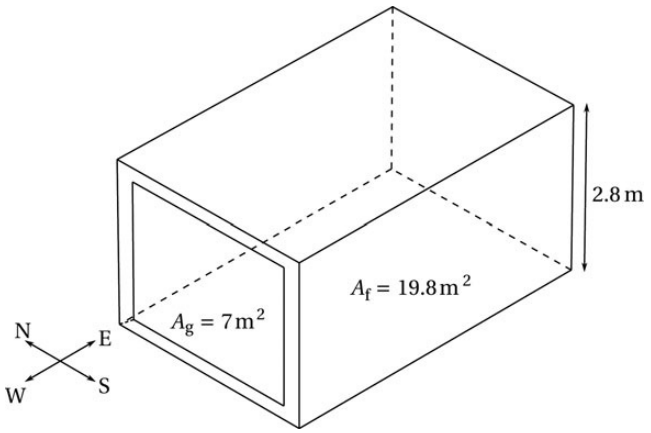

Figure 2. *Wire-frame drawing of office zone modelled.*

components. The thermal inertia of each component is determined by its heat capacity. The internal heat capacity per area of building element is determined using ISO 13786 [10]. The procedure is based on the solution of the one-dimensional heat diffusion equation in a homogeneous slab given in the following equation:

$$\frac{\partial^2 T}{\partial d^2} = \frac{\rho c}{\lambda}\frac{\partial T}{\partial t}. \qquad (1)$$

where T is thermodynamic temperature (in K).

For a finite slab subject to sinusoidal temperature variations this equation can be solved using matrix algebra [11]. The full set of equations, matrix set-up and procedure is provided in ISO 13786. This allows for the calculation of the thermal admittance and heat capacity of each building component. The thermal transmittance of the structure and roof was determined in accordance with ISO 6946 [12] using the thermophysical data.

The results of the model simulation for each of the test cases are given in Table 1. The calculated values are compared with the

Table 1. *Yearly values for heating and cooling energy needs with validation results.*

Test	$Q_{H,ref}$ (kWh)	$Q_{C,ref}$ (kWh)	$Q_{tot,ref}$ (kWh)	$Q_{H,calc}$ (kWh)	$Q_{C,calc}$ (kWh)	$Q_{tot,calc}$ (kWh)	rQ_H	rQ_C	Accuracy
5	463.1	201.7	664.8	452.9	200.7	653.7	0.0153	0.0015	Level A
6	509.8	185.1	694.9	517.0	179.3	696.2	0.0103	0.0084	Level A
7	1067.4	19.5	1086.9	1079.2	15.5	1094.8	0.0109	0.0036	Level A
8	313.2	1133.2	1446.4	309.5	1147.3	1456.8	0.0026	0.0097	Level A
9	747.1	158.3	905.4	766.4	147.4	913.8	0.0214	0.0121	Level A
10	574.2	192.4	766.6	571.5	181.6	753.1	0.0035	0.0141	Level A
11	1395.1	14.1	1409.2	1432.9	8.2	1441.1	0.0268	0.0042	Level A
12	533.5	928.3	1461.8	542.4	962.5	1504.9	0.0061	0.0234	Level A

reference values using the following equations:

$$rQ_H = \frac{abs(Q_{H,calc} - Q_{H,ref})}{Q_{tot,ref}} \tag{2a}$$

$$rQ_C = \frac{abs(Q_{C,calc} - Q_{C,ref})}{Q_{tot,ref}}. \tag{2b}$$

where $Q_{H,ref}$ is quantity of heating energy (in kWh, reference value), $Q_{C,ref}$ is the quantity of cooling energy (in kWh, reference value), $Q_{C,calc}$ is the calculated cooling energy (in kWh), $Q_{H,calc}$ is the calculated heating energy (in kWh).

Level of accuracy is graded with levels A, B and C. The validation tests are complied with if for each of the cases 5–12:

$$\begin{aligned} &\text{Level A}: \quad rQ_H \leq 0.05 \quad \text{and} \quad rQ_C \leq 0.05 \\ &\text{Level B}: \quad rQ_H \leq 0.10 \quad \text{and} \quad rQ_C \leq 0.10 \\ &\text{Level C}: \quad rQ_H \leq 0.15 \quad \text{and} \quad rQ_C \leq 0.15. \end{aligned}$$

This relation is used instead of a direct comparison (e.g. $Q_{C,calc}$ vs. $Q_{C,ref}$), because a relative difference of, say, 35% (as in Test Case 11) in this cooling requirement has no real meaning if the level of cooling required is negligible compared with the energy needed for heating, which is almost 100 times that in this case. This is also the basis on which the European Standard [8] calculates the accuracy of the dynamic model.

As can be seen from the results in Table 1, the model shows a high level of accuracy across all the validation tests, with *Level A* being reached for all eight cases.

With a baseline validated model comprising only five ODEs in a state-space form, a malleable framework is provided in which the equations can be modified in order to implement different servicing systems into the building model. This also delivers a model that can be used in state-space controller design procedures.

2.3 Micro-generation models

Extending the validated building model, the equations can be modified to include the CHP plant and the thermal energy store. The CHP is represented by a simplified energy-based model given by the following equation:

$$\phi_{CHP}(t) = \epsilon f_H \phi_{gas}(t), \tag{3}$$

where ϵ is the efficiency of the plant, f_H the fraction of fuel power converted to thermal power and ϕ_{gas} the controllable input of fuel into the engine or heat flow rate/thermal power (in W). It follows that the electrical power (P, in W) produced by the CHP engine is given by the following equation:

$$P_{CHP}(t) = \epsilon(1 - f_H)\phi_{gas}(t). \tag{4}$$

The thermal energy store model also uses an energy-based approach and is given by the following equation:

$$Q_{store}(t) = f_{CF} \int_{t_0}^{t} \phi_{store}(\tau) d\tau + Q_{store}(t_0), \tag{5}$$

where $\phi_{store}(t)$ is the amount of thermal power extracted from or supplied to the store at the current time step, $Q_{store}(t_0)$ is the value of the integral at the previous time step and f_{CF} is the conversion factor (W to kWh). This is required as the state of charge of the thermal energy store that is required by the controller. Substituting Equations (3) and (5) into Equation (A1), the thermal power supplied to the air node, $\phi_H(t)$, is given by

$$\phi_H(t) = \epsilon f_H \phi_{gas}(t) + \phi_{store}(t). \tag{6}$$

Both the CHP and thermal energy store have physical limitations that must be modelled to ensure they more closely resemble reality. The CHP engine will have a maximum fuel supply rate denoted by $\phi_{chp,max}$. The CHP engine modelled in this case is based upon a Free Piston Stirling Engine [13], which generates 6 kW of heat and 1 kW of electricity by driving a magnetic piston up and down within a generator coil. The unit can also modulate down to as low as 3 kW, while still generating electricity. The unit is capable of modulating its electrical output between 0.3 and 1.0 kW [13]. For these analyses it is assumed that the engine is capable of fully modulating between these two limits. Furthermore, a fixed efficiency and heat-to-power ratio is also assumed.

In addition, it is assumed that the thermal energy store is perfectly insulated from the zone. In reality, storage efficiencies can typically vary between 50 and 90%. The losses from the store, were it located in the zone, would act as an additional heat gain, which would have an effect on summer cooling loads.

The physical limits of the thermal store are numerous and the following are accounted for in the model. The maximum amount of heat it is able to absorb is equal to the amount of thermal energy being produced by the CHP engine, given by $-\epsilon f_H \phi_{gas}(t)$, since it cannot extract heat from the zone. Additionally, the

thermal store has a thermal energy capacity, Q_{cap}, where the correct sizing for the building zone modelled is determined using an iterative procedure given in Section 3.

2.4 Control strategy

The dynamic model of the building and its servicing systems are modelled in the time domain using a state-space representation. In order to get the equations into a state-space form, the system equations are linearised using the first-order term of the Taylor series expansion around the equilibrium conditions of the building.

$$\dot{\boldsymbol{x}}(t) = \boldsymbol{A}(t)\boldsymbol{x}(t) + \boldsymbol{B}\boldsymbol{u}(t) + \boldsymbol{F}(t)\boldsymbol{d}(t) \tag{7a}$$

$$\boldsymbol{y}(t) = \boldsymbol{C}\boldsymbol{x}(t) + \boldsymbol{D}\boldsymbol{u}(t) + \boldsymbol{G}\boldsymbol{d}(t), \tag{7b}$$

where $\dot{\boldsymbol{x}}(t) \in \mathbb{R}^n$ is the state vector, $\boldsymbol{u}(t) \in \mathbb{R}^m$ the input control vector, $\boldsymbol{d}(t) \in \mathbb{R}^q$ a disturbance vector, $\boldsymbol{y}(t) \in \mathbb{R}^p$ the output vector, $\boldsymbol{A} \in \mathbb{R}^{n\times n}$ the plant matrix, $\boldsymbol{B} \in \mathbb{R}^{n\times m}$ is input matrix, $\boldsymbol{C} \in \mathbb{R}^{p\times n}$ the output matrix, $\boldsymbol{D} \in \mathbb{R}^{p\times m}$ the feedforward matrix, $\boldsymbol{F} \in \mathbb{R}^{n\times q}$ the system disturbance matrix and $\boldsymbol{G} \in \mathbb{R}^{p\times q}$ the output disturbance matrix.

Note that the plant and system disturbance matrices are time varying due to the known change in the mechanical ventilation rate, and not due to a change in any of the state variables. This is evident from the system matrices given in Appendix A.2.

Equation (7b) is the output equation from which the controlled system variables can be found. In this system there are two outputs: (1) the operative temperature and (2) the electrical grid power. The operative temperature in this case is purely the air temperature of the zone, i.e.

$$y_1(t) = T_a(t). \tag{8}$$

The electrical grid power is given by

$$\begin{aligned} y_2(t) = P_{grid}(t) = P_{int}(t) + P_{led}(t) \\ - P_{bat}(t) - P_{pv}(t) - P_{chp}(t) \end{aligned} \tag{9}$$

where P_{int} is internal load power (in W), P_{led} lighting power (in W), P_{pv} photovoltaic power (in W).

It can be seen from Equation (9) that the availability of PV is considered a disturbance. In this way, priority is given to utilising as much of the PV-generated electricity as possible, while the electrically-led CHP can compensate for the remaining demand. The state-space vectors and matrices for the system can be found by substituting Equation (8), (9) and (A1) into the state-space form given by Equation (7). These are provided in Appendix A.2.

The control strategy employed uses nonlinear inverse dynamics controller design methods originally developed in the aerospace and robotics industry [14], and more recently applied to the controllability of buildings[7]. Known as robust inverse dynamics estimation (RIDE), this time-domain method, expressed in terms of state variables, is used to design a suitable compensation scheme for the control system.

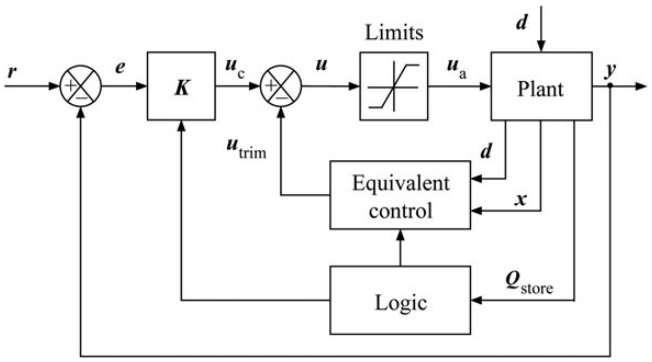

Figure 3. *RIDE control system schematic.*

As shown in Figure 3, the RIDE methodology comprised two control signals: (1) $\boldsymbol{U}_C$ (outer control loop compensator)—a function of the error between the reference input and the relative output and (2) $\boldsymbol{U}_{trim}$ (inner loop inverse dynamics control signal)—a function of the feedback of the system's current state and measured disturbance inputs. This allows the RIDE controller to compensate for the disturbance inputs and slow-building dynamics. This implementation of the RIDE control algorithm is based upon an 'ideal control philosophy' which aims to show whether, for a given design, ideal control is feasible while maintaining the stability of the system. However, it has been shown that by rapid estimation of the $\boldsymbol{U}_{trim}$ term, the RIDE control design methodology can be implemented in practice [7].

The control signal (in the Laplace domain) is given by

$$\boldsymbol{U} = \boldsymbol{U}_C + \boldsymbol{U}_{trim}, \tag{10}$$

where

$$\boldsymbol{U}_C = \boldsymbol{K}\boldsymbol{\Sigma}\boldsymbol{E}, \tag{11}$$

$$\boldsymbol{U}_{trim} = -\boldsymbol{K}[\boldsymbol{C}\boldsymbol{A}\boldsymbol{x} + (s\boldsymbol{G} + \boldsymbol{C}\boldsymbol{F})\boldsymbol{d}]. \tag{12}$$

where E is the error matrix.

The controller matrix $\boldsymbol{K} = (s\boldsymbol{D} + \boldsymbol{C}\boldsymbol{B})^{-1}$, and the decoupling matrix $\boldsymbol{\Sigma}$, is a diagonal matrix containing the design time constants for each control channel. This allows the control strategy to select a different time response for the tracked temperature and grid output.

The overall control strategy alternates between two RIDE control modes: (1) the 'default', for when the thermal store has space capacity and (2) for when it is saturated, i.e. 100% capacity. The controller signals are found by substituting the state-space matrices (as provided in Appendix A.2) into Equations (10)–(12). Taking the inverse Laplace transform and simplifying, the

Table 2. *Control mode combinatorial logic table.*

Logical tests			CHP inhibited
$Q_{store} = Q_{cap}$	$Q_{store} = Q_{cyc}$	Last action	
False	False	Not inhibited	False
False	False	Inhibited	True
False	True	Not inhibited	False
False	True	Inhibited	False
True	False	Not inhibited	True
True	False	Inhibited	True
True	True	Not inhibited	False
True	True	Inhibited	False

control signals for the default mode are given by

$$\phi_{gas}(t)|_{\phi_{min}}^{\phi_{max}} = K_{11}[(1/\tau_1)e_{temp}(t) - \sigma_1(t) - \sigma_2(t)] + K_{12}\left[(1/\tau_2)\int_{t_0}^{t} e_{grid}(t)|_{-\infty}^{0} - P_{load}(t)|_{0}^{\infty}\right] \quad (13)$$

$$\phi_{store}(t)|_{-\epsilon f_H \phi_{gas}}^{\phi_{max}} = K_{21}[(1/\tau_1)e_{temp}(t) - \sigma_1(t) - \sigma_2(t)] + K_{22}\left[(1/\tau_2)\int_{t_0}^{t} e_{grid}(t)|_{-\infty}^{0} - P_{load}(t)|_{0}^{\infty}\right] \quad (14)$$

$$P_{bat}(t) = K_{31}[(1/\tau_1)e_{temp}(t) - \sigma_1(t) - \sigma_2(t)] + K_{32}\left[(1/\tau_2)\int_{t_0}^{t} e_{grid}(t) - P_{load}(t)\right] \quad (15)$$

where

$$\sigma_1(t) = a_{11}T_a(t) + a_{12}T_{iw}(t) + a_{13}T_r(t) + a_{14}T_f(t) + a_{15}T_s(t)$$
$$\sigma_2(t) = e_{11}T_o(t) + e_{12}I_{sol}(t) + e_{13}I_{int}(t) + e_{14}I_{led}(t)$$
$$P_{load}(t) = P_{int}(t) + P_{led}(t) - P_{pv}(t)$$
$$\tau = \text{time constant}$$

When the store is full, it can no longer absorb the excess heat generated by the CHP to fulfil the electrical energy demand. Therefore, when the store is saturated, the control is switched to the CHP-inhibited state, where the CHP engine is not in operation and the control elements $K_{11} = K_{12} = K_{22} = K_{31} = 0$, $K_{21} = K_{21}^*$, and $K_{32} = K_{32}^*$. The elements of the controller matrix $\boldsymbol{K}$ are provided in Appendix A.2. The control mode switching is determined using the combinatorial logic table given in Table 2.

In the CHP-inhibited state, the store fulfils the heat demand, while the electrical demand will be met by the grid and spare capacity within the electrical energy storage. Note that the controller can operate without the need of any electrical energy storage, as shown in Section 3. It is designed to minimise the electrical grid use with whatever resources it has available.

The control logic contains a thermal energy store 'cycle capacity', which stops rapid mode switching around the maximum capacity of the store, as such, the cycle capacity should not be set to the maximum capacity of the store. Note that the combinatorial logic table must account for all logic combinations, even though such a scenario could cause instability. Therefore, the logic is configured such that the CHP would always be inhibited were the cycle capacity set to the maximum capacity of the store. The specific cycle capacity can be set on a case-by-case basis, but the results have shown improved energy performance at low (10–20% of maximum capacity) cycle capacities, as this leads to increased utilisation of the store.

2.5 Controllability

Analysis of the controller matrix $\boldsymbol{K}$ determines the circumstances under which the system would become uncontrollable. If $\boldsymbol{K}$ were to become zero or undefined then control of the system would be lost as it is a pre-multiplier of both $\boldsymbol{U}_c$ and $\boldsymbol{U}_{trim}$. Therefore, in order to ensure that the system can be controlled via the RIDE methodology, it is critical that $(\boldsymbol{sD} + \boldsymbol{CB})$ is invertible. This can either be a two-sided inverse in the case that $(\boldsymbol{sD} + \boldsymbol{CB})$ is square, otherwise for a general $(p \times m)$ matrix we must ensure that it has a right inverse (i.e. has full row rank). This can be done algebraically by ensuring that the following determinant is not equal to zero

$$|(\boldsymbol{sD} + \boldsymbol{CB})(\boldsymbol{sD} + \boldsymbol{CB})^{\mathrm{T}}| \neq 0. \quad (16)$$

The matrices $\boldsymbol{B}$, $\boldsymbol{C}$ and $\boldsymbol{D}$ are substituted into Equation (16) for the limiting case when there is no electrical battery storage available, which produce

$$\frac{\epsilon(f_H - 1)}{C_a} \neq 0. \quad (17)$$

Consequently, the following conditions exist for controllability by examining Equation (17):

- The CHP is operational, i.e. $\epsilon \neq 0$.
- A fraction of the gas input into the CHP engine is converted to electricity, i.e. $f_H \neq 1$.

Therefore, as long as the CHP engine is operational, and it simultaneously produces electricity and thermal energy, then the system will be controllable.

3 RESULTS AND DISCUSSION

3.1 Simulation parameters

The results given here are calculated using two reference inputs. The first is the operative temperature (in this case the air temperature of the zone). This heating set point is 20°C between 08:00 and 18:00 on weekdays, with a nighttime and weekend setback temperature of 12°C. The cooling has been disabled for these simulations in order to draw closer comparisons between different configurations that may not lend themselves to incorporating cooling, as such, a cooling device has not been included in this set of results. The second is the national grid power set point, which is set to zero. This means that the controller will strive to neither import or export from or to the national grid, thereby minimising the use of the grid.

The building zone modelled is Test 9 from Section 2.2, and retains the same climate data as before. The internal gains are defined per floor area at 20 W/m^2 and are defined as 50% convective to the internal air of the zone and 50% radiative to the walls and floor. The electrical loads comprised the internal gains, at 20 W/m^2, which equates to a standing load of 396 W between 08:00 and 18:00 during weekdays.

The energy production from PVs is calculated using PVWatts [15]. The PV system characteristics consist of a 650-W solar array, south facing with a fixed tilt of 48.73° (which is equal to the latitude of the climate data). In all simulations there was a total available power from PVs amounting to 538 kWh over the year.

The simulations here are idealised and consider the actuator to be a convective device that supplies heat directly to the internal air node. The sensor is also assumed to be located at the internal air node. The results are presented for the situation where there is no centralised electrical energy storage. This highlights that the controller is able to operate without any energy 'buffer' in the electrical network.

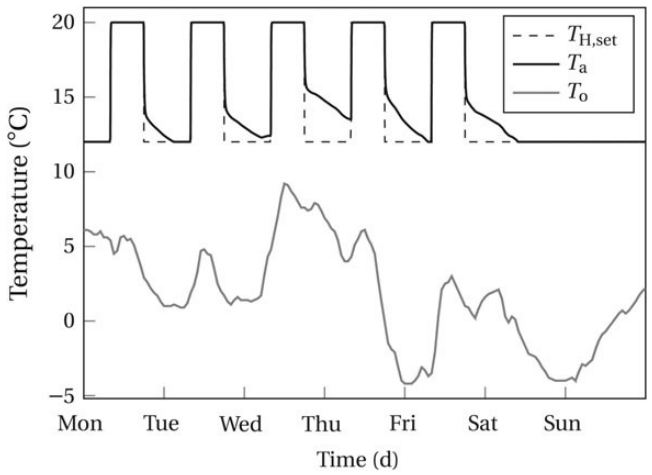

Figure 4. *Dynamic response—temperature.*

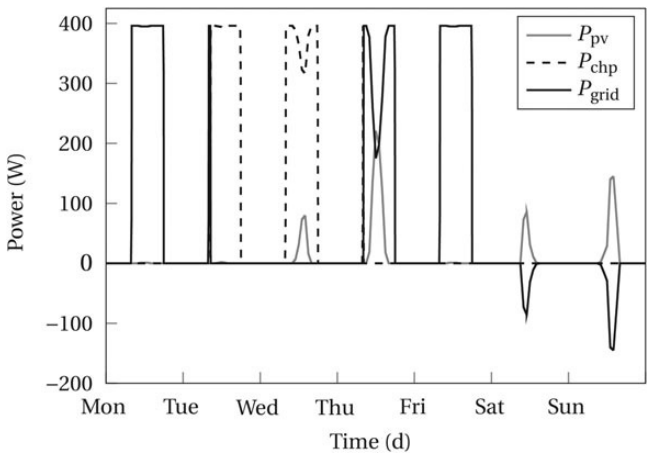

Figure 5. *Dynamic response— power.*

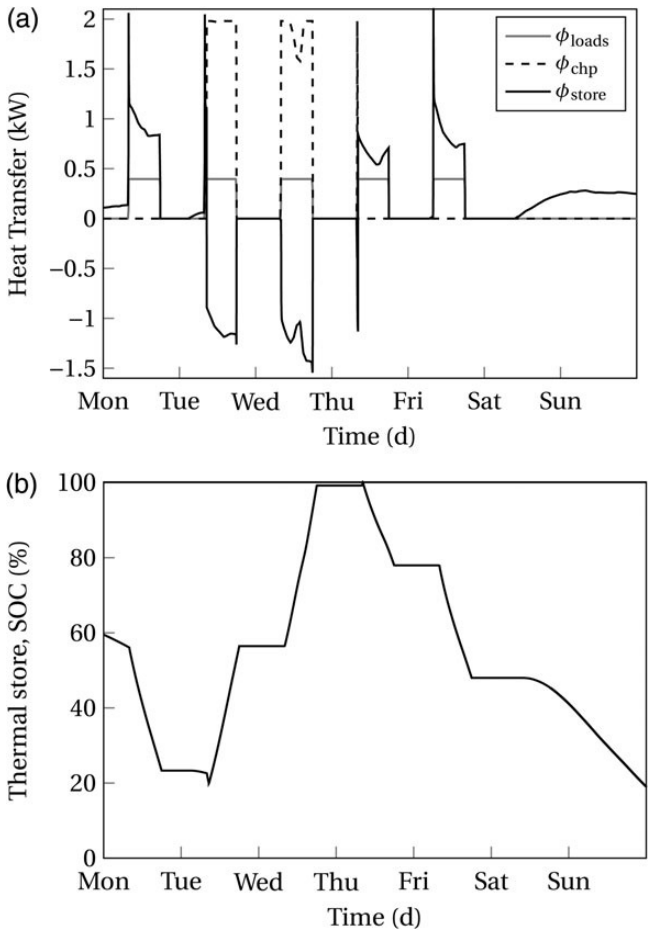

Figure 6. *Dynamic response—zone thermal energy. (a) Heat sources; (b) Thermal energy store.*

Table 3. *Energy and CO_2 emission comparison.*

System	Q_{gas} (kWh)	E_{grid} (kWh)	CO_2 (kg)
Condensing boiler	983.5	672.7	532.2
Air source heat pump	N/A	931.5	484.7
CHP and thermal store	1201.7	492.4	478.8

3.2 Simulation results

Figures 4–6 show the dynamic results from the model over the period of a week in December, where the update period for the control is set at 3.33 mHz (i.e. 5 min). Best performance is typically achieved when the update period is set four to five times faster than the slowest time constant in the system. Figure 4 displays the control algorithm's ability to maintain the set-point temperature with 'perfect tracking' during the hours 08:00 to 18:00. This is due to inverse dynamics control term U_{trim}, which compensates for the external disturbance changes such as external temperature or solar radiation that would typically cause fluctuation around the set point.

Table 3 shows the gas and electrical grid utilisation for the year for the model in comparison with several alternative

Table 4. *Thermal store sizing results.*

Q_{cap} (kWh)	Q_H (kWh)	Q_{gas} (kWh)	E_{grid} (kWh)	CO_2 (kg)
∞	896.0	4508.9	0.0	835.1
142.0	896.0	1124.7	507.6	472.4
56.9	896.0	1173.1	500.4	477.7
42.7	896.0	1175.9	500.0	478.0
28.5	896.0	1201.2	496.2	480.7
11.4	894.3	1199.6	496.4	480.5

systems. The results for the condensing boiler system are based upon a high efficiency grade A unit with a seasonal efficiency of 91.1%. The air source heat pump results are calculated using a previously published methodology [16].

The CO_2 emissions for each system are calculated using the latest emission factors from Defra (updated 31 May 2012). The results show that the CHP and thermal store model effectively reduces the use of the national grid and consequently reduces the CO_2 emissions over the other systems.

The electrical loads in the office amount to 396 W between 08:00 and 18:00, resulting in an annual load of 1033.6 kWh (261 operational days/year). The PV system provides 538 W over the year, of which 360.9 kWh are utilised, which amounts to 34.9% of the annual load. The CHP provides an additional 180.2 kWh of electrical energy, amounting to 17.5% of the annual load. This is all the while minimising the CHP's export to the grid, with 0 kWh being exported to the grid due to the electrically led CHP.

The model can be used to size the thermal energy store for the particular building zone modelled by using an iterative design procedure. The model begins with an infinite thermal energy capacity in order to determine the heat and electrical demands of the building zone over a simulated year. It then reduces the size of the thermal store incrementally until the heating set point cannot be met, indicating the store does not have a sufficient thermal energy capacity. Table 4 highlights the influence of the size of the store on the energy performance of the building zone.

Results indicate that the 11.4 kWh thermal energy store, which for a wet system would approximate to a 200 l water storage tank, is undersized for this building zone. This is because it is unable to deliver the required thermal energy over the year, 896.0 kWh, which is calculated using the infinite thermal energy store.

The results also show that generally, the larger the thermal store the lower the overall energy consumption and CO_2 emissions. However, with an idealised infinite thermal store, the total energy supplied and resultant CO_2 emissions are higher than the stores with a fixed thermal capacity. This is because the controller will always use the CHP to meet both the thermal and electrical demands over the year, and dumps the excess thermal energy produced into the store which is never fed back into the system.

4 CONCLUSION AND FUTURE WORK

A simplified dynamic building physics model with energy performance results validated with EN 15265 has been presented. The validity of the modelling approach taken has been highlighted in this paper. This research confirms that it is possible to run an electrically led CHP system, with a coupled thermally/electrically led thermal energy store. Modifications were made to the building model to allow for the simplified implementation of energy-based models for a CHP plant and thermal energy store. The flexibility of this modelling approach is highlighted by the simplicity of adding the aforementioned systems into the model. It has also been demonstrated that the sizing of the thermal energy store is an optimisation problem that could be expanded on in the future.

The modelling approach provided here could be followed by other dynamic models wishing to validate with international standards. This approach could also extend methods such as the Simplified Building Energy Model (SBEM) [4, 17] by simply estimating the potential transient impact of innovative technologies to energy estimation and regulation. SBEM is used as a compliance tool for building regulations for non-domestic buildings in the UK. However, SBEM cannot be used to assess advanced dynamic controllability such as the model presented here. The modelling environment presented here suggests that a move towards more dynamic modelling for energy estimation, controller design and regulatory compliance could be beneficial.

Using this methodology, other heating systems such as standard wet systems and air supply systems can be modelled and compared with a more complex heating scenario such as CHP. Additionally, since the controller is also capable of managing electrical energy storage, the potential carbon reduction and grid use reduction resulting from this could be investigated for a number of micro-generation technology configurations. This can be used to suggest the energy benefit gained from a building changing its heating system. Energy savings generated by this model can be monetised and used as a basis to suggest the payback period for a building to upgrade its heating system.

The modelling environment could be amended to more closely model real life. For example, state estimation can be added to the U_{trim} parameter to determine controller performance that is closer to reality.

The controller presented here is based upon inverse dynamics. Alternative controllers can be assessed using this building model. An interesting area of future work would be to compare the RIDE controller with a more simplistic controller to gauge the benefit of advanced control on a building's energy use.

Controllable lighting can be taken into account within the model. On average lighting accounts for 32% of the electrical energy use in commercial buildings in the UK [18], more than double that of the computing devices (15%). Controllability of lighting is an area of exciting future research—using this modelling approach it can be determined whether it is possible to control lighting to help ensure more autonomous behaviour in buildings.

FUNDING

This research was funded by the BRE Trust as part of the University of Strathclyde's BRE Centre of Excellence in Energy Utilisation and in partnership with an EPSRC research grant.

REFERENCES

[1] Clarke J, Johnstone C, Kelly N, *et al*. The role of built environment energy efficiency in a sustainable UK energy economy. *Energ Policy* 2008;**36**: 4605–9.

[2] European Construction Technology Platform & European Commission. Challenging and changing Europe's built environment. A vision for a sustainable and competitive construction sector by 2030. Technical report, 2005. http://www.ectp.org/documentation/ECTP-Vision2030-25Feb2005.pdf.

[3] Energy Efficiency in Buildings & World Business Council for Sustainable Development. Transforming the market: energy efficiency in buildings. Technical report, 2009. http://www.wbcsd.org/transformingthemarketeeb.aspx.

[4] Tuohy P, Davis Langdon LLP, The Scottish Government & Building Standards Division. Benchmarking Scottish energy standards: Passive House and CarbonLite Standards: a comparison of space heating energy demand using SAP, SBEM, and PHPP methodologies. Technical report, 2009. http://www.scotland.gov.uk/Resource/Doc/217736/0091333.pdf.

[5] Feist W. Certified passive house—criteria for non-residential passive house buildings, 2012. http://passiv.de/downloads/03_certfication_criteria_nonresidential_en.pdf.

[6] Mago PJ, Hueffed A, Chamra LM. Analysis and optimization of the use of CHP-ORC systems for small commercial buildings. *Energy Build* 2010;**42**:1491–8. doi:10.1016/j.enbuild.2010.03.019.

[7] Counsell J, Khalid Y, Brindley J. Controllability of buildings: a multi-input multi-output stability assessment method for buildings with slow acting heating systems. *Simul Model Pract Theory* 2011;**19**:1185–200. doi:10.1016/j.simpat.2010.08.006.

[8] British Standards Institution. BS EN 15265: Energy performance of buildings. Calculation of energy needs for space heating and cooling using dynamic methods. General criteria and validation procedures. British Standards Institution, 2007.

[9] Murphy GB, Counsell J, Allison J, *et al*. Calibrating a combined energy systems analysis and controller design method with empirical data. *Energy* 2013;**57**:484–94. doi:10.1016/j.energy.2013.06.015.

[10] British Standards Institution. BS EN ISO 13786: Thermal performance of building components. Dynamic thermal characteristics. Calculation methods. British Standards Institution, 2007.

[11] Pipes L. Matrix analysis of heat transfer problems. *J Franklin Inst* 1957;**263**:195–206. doi:10.1016/0016-0032(57)90927-4.

[12] British Standards Institution. BS EN ISO 6946: Building components and building elements. Thermal resistance and thermal transmittance. Calculation method, 2007.

[13] Baxi. The baxi ecogen dual energy system, 2012. http://www.baxiknowhow.co.uk/documents/Baxi-Ecogen-consumer-brochure.pdf.

[14] Bradshaw A, Counsell J. Design of autopilots for high performance missiles. *Proc Inst Mech Eng, Part I: J Syst Control Eng* 1992;**206**:75–84. doi:10.1243/pime_proc_1992_206_313_02.

[15] National Renewable Energy Laboratory. PVWatts, 2012. http://rredc.nrel.gov/solar/calculators/PVWATTS/version1/.

[16] Murphy G, Counsell J, Baster E, *et al*. Symbolic modelling and predictive assessment of air source heat pumps. *Build Serv Eng Res Technol* 2013;**34**: 23–39. doi:10.1177/0143624412462592.

[17] Hitchin R. *A Guide to the Simplified Building Energy Model (SBEM): What It Does and How It Works*. HIS BRE Press, 2010. ISBN 978-1-84806-129-3.

[18] Department of Energy & Climate Change. Energy consumption in the UK, Table 5.6a. Technical Report URN 12D/272, 2012. https://www.gov.uk/government/uploads/system/uploads/attachment_data/file/65959/271-ecuk-service-2010.xls.

APPENDIX

A.1 BUILDING MODEL EQUATIONS

$$\begin{aligned} C_a \dot{T}_a(t) = &-(H_g + H_{ni} + H_v(t) + H_{iw} + H_r \\ &+ H_f + H_s)T_a(t) + H_{iw}T_{iw}(t) \\ &+ H_r T_r(t) + H_f T_f(t) + H_s T_s(t) \\ &+ (H_g + H_{ni} + H_v(t))T_o(t) \\ &+ f_{sa}A_{sol}I_{sol}(t) + f_{int,c}A_f I_{int}(t) \\ &+ f_{int,c}A_f I_{led}(t) + \phi_{HC}(t) \\ &- A_{sky}T_{sky}(t) \end{aligned} \tag{A.1}$$

where H_v is ventilation heat transfer coefficient (in W/K), H_{ni} natural infiltration heat transfer coefficient (in W/K), H_{rad} radiative heat transfer coefficient (in W/K), A_{sol} solar area (in m^2), I_{int} total heat flux from internal sources (in W/m^2), I_{sol} solar irradiance ($W\ m^2$), f_{sa} is the fraction of solar flux directly acting on the internal air node

$$\begin{aligned} C_{iw}\dot{T}_{iw}(t) = &H_{iw}T_a(t) - (H_{iw} + H_{rad,iw-r} \\ &+ H_{rad,iw-f} + H_{rad,iw-s})T_{iw}(t) \\ &+ H_{rad,iw-r}T_r(t) + H_{rad,iw-f}T_f(t) \\ &+ H_{rad,iw-s}T_s(t) + f_{ss}f_{df,iw}A_{sol}I_{sol}(t) \\ &+ f_{int,iw}f_{int,rad}A_f I_{int}(t) \\ &+ f_{int,iw}f_{int,rad}A_f I_{led}(t) \\ &- f_{ss}f_{df,iw}A_{sky}T_{sky}(t) \end{aligned} \tag{A.2}$$

where f_{ss} is the fraction of solar flux imparted on the internal surfaces

$$\begin{aligned} C_r\dot{T}_r(t) = &H_r T_a(t) + H_{rad,iw-r}T_{iw}(t) \\ &- (H_r + U_r^* A_r + H_{rad,iw-r} + H_{rad,r-f} + H_{rad,r-s})T_r(t) \\ &+ H_{rad,r-f}T_f(t) + H_{rad,r-s}T_s(t) + U_r^* A_r T_o(t) \\ &+ (f_{ss}f_{df,r}A_{sol} + g_r A_r)I_{sol}(t) \\ &- f_{ss}f_{df,r}A_{sky}T_{sky}(t) \end{aligned} \tag{A.3}$$

$$\begin{aligned} C_f\dot{T}_f(t) = &H_f T_a(t) + H_{rad,iw-f}T_{iw}(t) \\ &- (H_f + H_{rad,iw-f} + H_{rad,r-f} + H_{rad,r-s})T_f(t) \\ &+ H_{rad,r-f}T_r(t) + H_{rad,f-s}T_s(t) \\ &+ f_{ss}f_{df,f}A_{sol}I_{sol}(t) \\ &+ f_{int,f}f_{int,rad}A_f I_{int}(t) + f_{int,f}f_{int,rad}A_f I_{led}(t) \\ &- f_{ss}f_{df,f}A_{sky}T_{sky}(t) \end{aligned} \tag{A.4}$$

$$
\begin{aligned}
C_s \dot{T}_s(t) = {} & H_s T_a(t) + H_{rad,iw-s} T_{iw}(t) \\
& + H_{rad,r-s} T_r(t) + H_{rad,f-s} T_f(t) \\
& - (H_s + U_s^* A_s + H_{rad,iw-s} + H_{rad,r-s} + H_{rad,f-s}) T_s(t) \\
& + U_s^* A_s T_o(t) + (f_{ss} f_{df,s} A_{sol} + g_s A_s) I_{sol}(t) \\
& + f_{int,s} f_{int,rad} A_f I_{int}(t) + f_{int,s} f_{int,rad} A_f I_{led}(t) \\
& - f_{ss} f_{df,s} A_{sky} T_{sky}(t)
\end{aligned} \tag{A.5}
$$

A.2 STATE-SPACE MATRICES

$$
\boldsymbol{x} = \begin{bmatrix} T_a & T_{iw} & T_r & T_f & T_s \end{bmatrix}^T
$$

$$
\boldsymbol{u} = \begin{bmatrix} \phi_{gas} & \phi_{store} & P_{bat} \end{bmatrix}^T
$$

$$
\boldsymbol{d} = \begin{bmatrix} T_o & I_{sol} & I_{int} & I_{led} & P_{pv} & T_{sky} \end{bmatrix}^T
$$

$$
\boldsymbol{A} = \begin{bmatrix} a_{11}(t) & a_{12} & a_{13} & a_{14} & a_{15} \\ a_{21} & a_{22} & a_{23} & a_{24} & a_{25} \\ a_{31} & a_{32} & a_{33} & a_{34} & a_{35} \\ a_{41} & a_{42} & a_{43} & a_{44} & a_{45} \\ a_{51} & a_{52} & a_{53} & a_{54} & a_{55} \end{bmatrix} \quad \boldsymbol{B} = \begin{bmatrix} b_{11} & b_{12} & 0 \\ 0 & 0 & 0 \\ 0 & 0 & 0 \\ 0 & 0 & 0 \\ 0 & 0 & 0 \end{bmatrix}
$$

$$
\boldsymbol{C} = \begin{bmatrix} 1 & 0 & 0 & 0 & 0 \\ 0 & 0 & 0 & 0 & 0 \end{bmatrix} \quad \boldsymbol{D} = \begin{bmatrix} 0 & 0 & 0 \\ d_{21} & 0 & -1 \end{bmatrix}
$$

$$
\boldsymbol{F} = \begin{bmatrix} f_{11}(t) & f_{12} & f_{13} & f_{14} & 0 & f_{16} \\ 0 & f_{22} & f_{23} & f_{24} & 0 & f_{26} \\ f_{31} & f_{32} & 0 & 0 & 0 & f_{36} \\ 0 & f_{42} & f_{43} & f_{44} & 0 & f_{46} \\ f_{51} & f_{52} & f_{53} & f_{54} & 0 & f_{56} \end{bmatrix}
$$

$$
\boldsymbol{G} = \begin{bmatrix} 0 & 0 & 0 & 0 & 0 \\ 0 & 0 & g_{23} & g_{24} & -1 \end{bmatrix}
$$

$$
\boldsymbol{K} = \begin{bmatrix} K_{11} & K_{12}\dfrac{1}{s} \\ K_{21} & K_{22}\dfrac{1}{s} \\ K_{31} & K_{32}\dfrac{1}{s} \end{bmatrix}
$$

and

$$
\begin{aligned}
K_{11} &= \frac{b_{11}}{\kappa} & K_{12} &= \frac{b_{12}^2 d_{21}}{\kappa} \\
K_{21} &= \frac{(d_{21}^2 + 1) b_{12}}{\kappa} & K_{22} &= -\frac{b_{11} b_{12} d_{21}}{\kappa} \\
K_{31} &= \frac{b_{11} d_{21}}{\kappa} & K_{32} &= -\frac{b_{11}^2 + b_{12}^2}{\kappa} \\
K_{21}^* &= 1/b_{12} & K_{32}^* &= -1
\end{aligned}
$$

where

$$
\kappa = b_{11}^2 + (d_{21}^2 + 1) b_{12}^2
$$